CONEM 2022
CONGRESSO NACIONAL DE ENGENHARIA MECÂNICA
TERESINA - PI

ABCM

XI CONGRESSO NACIONAL DE ENGENHARIA MECÂNICA
DE 07 A 11 DE AGOSTO DE 2022, TERESINA-PI, BRASIL

TORSIONAL VIBRATION ANALYSIS ON RECIPROCATING COMPRESSORS

Tiago José de Menezes Cardoso, tiagojosemc@hotmail.com[1]
Aline Souza de Paula, alinedepaula@unb.br[1]

[1]Universidade de Brasília, Campus Universitário Darcy Ribeiro, Faculdade de Tecnologia, Asa Norte, CEP 70.910-900, Brasília-DF

Abstract: *Mechanical vibrations are associated with several reciprocating machine component problems. Internal combustion engines and reciprocating compressors are considered examples of this kind of machine. One of the most important mechanisms in reciprocating machines is the crankshaft, which may be considered the spinal column of these apparatuses. This rotating component can be affected by dynamic forces that work periodically and cause high-stress levels associated with vibrations that could originate leaks and fatigue failures. To understand better the phenomenon of vibrations in power transmission rotating systems of reciprocating compressors, a nonlinear mathematical model for torsional vibrations is presented for this sort of system. A system of four slider-crank mechanisms and an electric motor is presented. This structure is analyzed in order to identify its more significant differences when compared with a linear model. Critical conditions are found, and the system's dynamical response is observed for analysis.*
Keywords: *reciprocating machines, torsional vibrations, dynamics, nonlinearities*

1. INTRODUCTION

The slider-crank mechanism is one of the most crucial mechanical elements in machines such as reciprocating compressors (RCs). This sort of compressor converts rotational motion into linear motion, and this activity is done by the crankshaft, one of the leading mechanical components found in alternating machines. A crankshaft is a power transmission element that consists of a metal shaft with a series of cranks attached to connecting rods, and this whole aggregation of elements performs as an array of slider-crank mechanisms.

Excessive rotating flexural loads, high temperatures, and high-pressure levels are some of the conditions RCs are commonly exposed to and, as a consequence, important mechanical components such as their crankshafts also often experience drastic work conditions. For these reasons, failures are frequent. Mechanical vibrations constitute a significant factor in this scenario and they may be intensified by unbalanced loads significant enough to affect component lifetimes (Aliakbari *et al.*, 2018). A wide variety of faults related to mechanical vibrations occur in reciprocating machines. Excessive vibration problems often happen when the resonance frequencies of RC components are excited. Situations of this kind can also lead to adversities in different RC structural elements such as the casing, the foundation, and the anchoring system. The consequences of excessive vibrations can also reach other essential elements, such as the crankpins and their bearings, which also affect the machine's safety and reliability (Wachel and Tison, 1994).

Many authors developed different models to study mechanical vibrations in this sort of machine, considering specific non-linear system characteristics to represent more realistic phenomena. Metallidis and Natsiavas (2003) present dynamic models of RCs, taking into account the varying slider-crank mechanism moment of inertia and the driving and resisting torques as functions of the crankshaft motion which adds non-linearities to the model. Huang *et al.* (2012) also considers non-linear factors in his model, such as the non-constant inertia of reciprocating components and the structural damping of shaft segments. Pasricha and Carnegie (1979) formulate dynamic equations of motion for a multi-cylinder engine, allowing variable inertia in order to predict phenomena such as the secondary resonance, which scientists cannot predict with linear models. Brusa *et al.* (1997) studied the torsional vibration of crankshafts considering the variation of the geometry of the system with the crank angle and obtained more precise natural frequencies at the cost of increasing the size of the eigenproblem to be solved.

The present work presents a nonlinear model that represents an RC crankshaft. It considers variable inertia similarly to the models presented by Huang *et al.* (2012) and Metallidis and Natsiavas (2003). It represents an alternating compressor with four slider-crank mechanisms and an electric motor, which means it has five degrees of freedom (DOF).

2. PROBLEM DESCRIPTION

According to Metallidis and Natsiavas (2003), the physical model used to represent a reciprocating machine consists of two parts: the first is an association of slider-crank mechanisms, which are the actual resistive elements in a compressor; the second is the load, in the case the alternating machine is an engine, or an electric motor, in the case it is a compressor. In this last context, the motor is responsible for generating power to be used to compress gas by the slider-crank mechanisms. Both parts can be seen in Fig.1, which shows a simplified RC crankshaft representation with its main aspects. The model presented in this study also considers a flywheel (I_v) by the crankshaft's left end, as does Metallidis and Natsiavas (2003).

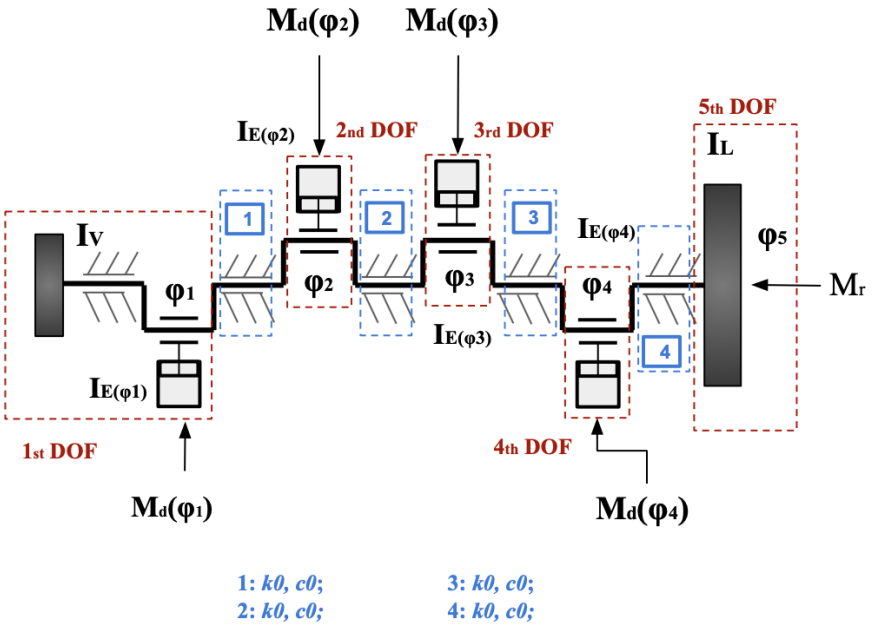

Figura 1: **Equivalent model for a reciprocating compressor with four cylinders.**

As shown in Fig. 1, there are four similar inertia elements in the center of the image, a more prominent inertia element on the right and a minor inertia element on the left, which is the flywheel. All of them are connected to a mutual shaft. Consequently, the motor (on the right) gives energy to the rest of the system, and the other elements use this energy to operate. The slider-crank mechanisms particularly react with resistive torque. I_E represents the variable inertia related to each RC individual slider-crank mechanism, according to Metallidis and Natsiavas (2003)' model, which is replicated here. I_L is the electric motor's inertia, I_V represents the flywheel's inertia, and ϕ_n is the angular displacement related to each DOF. All the angular displacement parameters are independent of one another. k_0 and c_0 are the stiffness and damping coefficients related to the shaft sections that connect inertia elements, except for the flywheel, which is considered rigid to the first crank. M_d and M_r are respectively the resistive torques that occur in the RC and the motor's generative torque. Last, c_e and c_l are additional damping elements related to individual DOF(s). They are not shown in Fig. 1 due to the excess of elements in the image, but they work as damping elements whose forces only depend on singular DOF velocities, as can be seen in the motion equations represented by Eq(s). 5 to 9.

2.1 Derivation of variable inertia for a single slider-crank mechanism

A slider-crank mechanism can be described as a composition of mechanical elements used to convert linear motion into rotary motion or vice-versa. At the same time the crank rotates along its axis, the piston performs a reciprocating movement due to the connecting rod's action (Huang *et al.* (2012)). When the alternating machine is a compressor, the crank converts rotational kinetic energy into linear motion used by the slider to move. A representation of this mechanism is shown in the Fig. 2. A shaft transmits torque T_m to the crank, and, as a consequence, the piston receives a resistive force F_p from the fluid it compresses. This force varies over time and depends on the independent crank's angular displacement ϕ_1. The angle between the dashed horizontal axis shown in Fig. 2 and the connecting rod is β, and the crank length is r. Last, the connecting rod length is l, and the length between the link represented by the letter L and the connecting rod's center of mass, represented by the letter G, is l_G.

Considering the crankpin's inertia is variable, a nonlinear equation gives the total kinetic energy of the mechanical system:

$$E_c = \frac{1}{2}\{I_c + m_1 r^2 + I_2\kappa^2(\phi_1) + (m_2 + m_p)r^2\sin^2(\phi_1)[1 + \kappa(\phi_1)]^2\}\dot{\phi_1}^2. \quad (1)$$

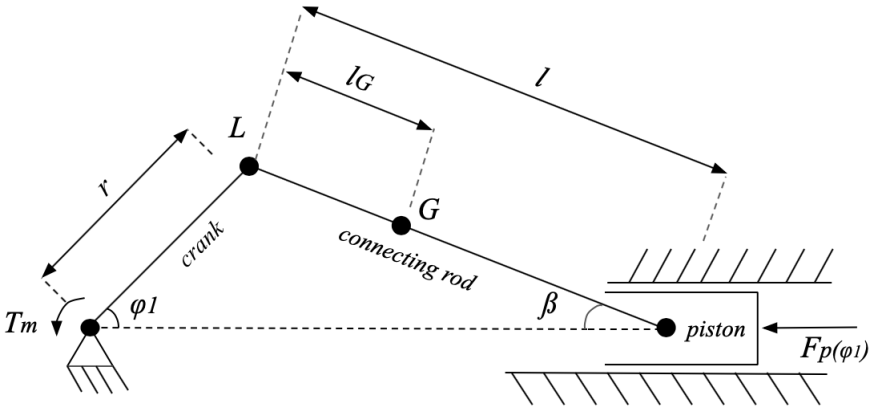

Figura 2: **Representation of slider-crank mechanism.**

In Eq. (1), I_c is the crank's inertia, m_1 is the mass associated with the connecting rod's section between its center of mass and the piston link, m_2 is the mass associated with the section between points L and G shown in Fig. 2 and m_p is the piston's mass. The expressions for $\kappa(\phi_1)$ and I_2 are given by Eq. (2) and Eq. (3), where I_G is the connecting rod's center of mass inertia and $\lambda = r/l$.

$$I_2 = I_G - m_1 l_G^2 - m_2(l - l_G)^2. \tag{2}$$

$$\kappa(\phi_1) = \frac{\lambda \cos(\phi_1)}{\sqrt{1 - \lambda^2 \sin^2(\phi_1)}}. \tag{3}$$

Considering the kinetic energy expression is given by $E_c = \frac{1}{2} I_E(\phi_1) \dot{\phi_1}^2$, it can be concluded from Eq. (1) that the mechanism's inertia is equal to:

$$I_E = I_c + m_1 r^2 + I_2 \kappa^2(\phi_1) + (m_2 + m_p) r^2 \sin^2(\phi_1)[1 + \kappa(\phi_1)]^2. \tag{4}$$

When considering a mechanical system with more than one slider-crank mechanism, it is necessary to consider the crankshaft set-up and the pistons' work sequence. In a crankshaft, the cranks and pistons are positioned in a specific arrangement to assure each piston will work in a particular order. The moment the first cylinder experiences a period of compression, for example, a different cylinder will probably be experiencing a different stage from the compressor's cycle, which includes suction, compression, expansion, and exhaust. These stages are related to the physical events the fluid inside a compressor's cylinder goes through when operating. The model presented by Metallidis and Natsiavas (2003) considers these aspects by introducing to the model the phase difference between the angular position of the first and the nth cylinder (γ_n) and the phase difference between the pistons' load angles (β_n). In order to replicate the model used by Metallidis and Natsiavas (2003), the values for γ_n considered in this study were $\gamma_1 = \gamma_4 = 0$ and $\gamma_2 = \gamma_3 = \pi$. For β, they were $\beta_1 = 0$, $\beta_2 = 3\pi$, $\beta_3 = \pi$ and $\beta_4 = 2\pi$. If the potential energy related to the presented system is obtained and the Lagrangian equations of motion are applied to the structure presented previously, which contains five DOF(s), the equations that rule the dynamics of this system can be obtained. However, according to Pesce *et al.* (2006), these equations cannot be applied directly to systems where mass varies unequivocally with angular displacement. Even in simple physical phenomena and not considering non-conservative generalized forces, the result is the formulation of motion equations with excess or absence of terms similar to $1/2(\partial m/\partial q)\dot{q}^2$, where q is the generalized coordinate used in Lagrange's equations. As a result, the term $1/2$ needs to be removed from the final motion equations. Finally, the equations that describe the system's dynamics are achieved.

$$(I_E(\phi_1) + I_V)\ddot{\phi_1} + \frac{dI_E(\phi_1)}{d\phi_1}\dot{\phi_1}^2 + c_0(\dot{\phi_1} - \dot{\phi_2}) + c_E\dot{\phi_1} + k_0(\phi_1 - \phi_2) = -M_d(\phi_1) \tag{5}$$

$$I_E(\phi_2 - \gamma_2)\ddot{\phi_2} + \frac{dI_E(\phi_2 - \gamma_2)}{d\phi_2}\dot{\phi_2}^2 + c_0(\dot{\phi_2} - \dot{\phi_1}) + c_0(\dot{\phi_2} - \dot{\phi_3}) + c_E\dot{\phi_2} + ...$$

$$... + k_0(\phi_2 - \phi_1) + k_0(\phi_2 - \phi_3) = -M_d(\phi_2 - \beta_2) \tag{6}$$

$$I_E(\phi_3 - \gamma_3)\ddot{\phi_3} + \frac{dI_E(\phi_3 - \gamma_3)}{d\phi_3}\dot{\phi_3}^2 + c_0(\dot{\phi_3} - \dot{\phi_2}) + c_0(\dot{\phi_3} - \dot{\phi_4}) + c_E\dot{\phi_3} + ...$$

$$... + k_0(\phi_3 - \phi_2) + k_0(\phi_3 - \phi_4) = -M_d(\phi_3 - \beta_3) \tag{7}$$

$$I_E(\phi_4 - \gamma_4)\ddot{\phi_4} + \frac{dI_E(\phi_4 - \gamma_4)}{d\phi_4}\dot{\phi_4}^2 + c_0(\dot{\phi_4} - \dot{\phi_3}) + c_0(\dot{\phi_4} - \dot{\phi_5}) + c_E\dot{\phi_4} + ...$$

$$... + k_0(\phi_4 - \phi_3) + k_0(\phi_4 - \phi_5) = -M_d(\phi_4 - \beta_4) \tag{8}$$

$$I_L\ddot{\phi_5} + c_0(\dot{\phi_5} - \dot{\phi_4}) + c_L\dot{\phi_5} + k_0(\phi_5 - \phi_4) = M_r \tag{9}$$

2.2 Cylinder resistive and driving torques

According to Metallidis and Natsiavas (2003), in engines, the torque used to drive the crankshaft results from the force exerted by the gas mixture on each engine cylinder. However, when the slider-crank mechanism to be analyzed is taken from a reciprocating compressor, its dynamical analysis shows that the force $F_p(\phi_n)$ results from the motion caused by the torque the electric motor delivers to the crankshaft. This force emerges as a reaction when the gas inside the piston's cylinder is compressed. This force can be calculated by subtracting the atmospheric pressure P_{atm} from the instantaneous pressure inside the piston p and multiplying the result by the cylinder's cross-sectional area A_c.

$$F_p(\phi_n) = (p - P_{atm})A_c. \tag{10}$$

Usually, the calculation process used to find this pressure is complex and involves solving coupled equations that can only be found by applicating simultaneous thermodynamic and dynamic laws (Metallidis and Natsiavas (2003), Heywood (1998), Dinca *et al.* (1999), Lyshevski (2000)). Yet, for the current work, it was considered sufficient to analyze the studied scenario as an ideal thermodynamical cycle from a four-stroke cycle engine (Heywood (1998), Dinca *et al.* (1999), Lyshevski (2000), Nisbeth and Budynas (1989)). As the studied machine is a compressor, the generative and resisting forces come from different sources, but the thermodynamical cycle can be considered the same. This assumption has, as a result, the use of the polytropic law to describe the compression and the expansion strokes. For this reason, Eq. (11) is valid in this scenario. In this expression, V is the varying volume the gas fills within the cylinder, and k is the adiabatic expansion coefficient, which depends on the gas being compressed. For air, which is the substance being considered in this study, this number is equal to 1.4. Volume can be obtained by Eq. (12), as follows.

$$p(V(\phi_n))^k = constant. \tag{11}$$

$$V(\phi_n) = V_c + [r + l - x_p(\phi_n)]\frac{\pi D_p^2}{4}. \tag{12}$$

V_c represents the cylinder's clearance volume and D_p its bore (cylinder's diameter). x_p is the piston's displacement. It is still necessary to determine V_c, whose expression is given by Eq. (13), where S_p is the total length the piston moves from the top dead center to its bottom dead center and R_c is the pump's compression ratio.

$$V_c = \frac{\pi}{4}\left(\frac{D_p^2 S_p}{R_c - 1}\right). \tag{13}$$

The instantaneous pressure is defined by Eq. (11), considering the gas is under compression when ϕ_1 varies from 0 to 0.771 radians and under expansion along with the interval from π to 5,362 radians. Although the same equation calculates the pressure in both scenarios, both volume and constant used in expression 11 are different in these two cycle phases, which results in different pressure curves. From 0.771 to π radians, the exhaust stage occurs at a certain fixed pressure, and the same happens from 5,362 to π radians during suction at the atmospheric pressure. Cylinders 1 and 4 perform their

thermodynamical cycles simultaneously, while cylinders 2 and 3 do the same with a phase difference of π radians from cylinders 1 and 4.

Finally, the resistive torque can be determined by Eq. (14), where K_x is the piston's speed coefficient given by Eq. (15).

$$M_d(\phi_n) = -K_x F_p(\phi_n). \tag{14}$$

$$K_x = -r[\sin(\phi_n) + \cos(\phi_n)\tan(\beta)]. \tag{15}$$

By substituting Eq. (10) and Eq. (15) in Eq. (14), the final resistive torque expression is determined.

$$M_d(\phi_n) = r[\sin(\phi_n) + \cos(\phi_n)\tan(\beta)](p - P_{atm})A_c. \tag{16}$$

The generative torque expression used in the reciprocating compressor model presented here comes from the curve shown in Doughty (1988), which presents how an induction motor's torque performs when its shaft rotational speed increases. For a specific velocity range, the torque produced by the motor decreases linearly. It happens in induction motors when the instantaneous speed gets close to its synchronous velocity and, for this reason, the equation used to express the generative electric torque is:

$$M_r = C_0 + C_1\dot{\phi_5}. \tag{17}$$

C_0 is the y-intercept of the curve obtained by Eq. (17) and C_1 is called its slope. The parameter C_0 will be especially important in this study as it can be used to control the amount of energy the motor delivers to the crankshaft, which means critical conditions can be found by choosing particular numbers for C_0.

2.3 Dimensionless equations of motion

Metallidis and Natsiavas (2003) suggest equivalent dimensionless dynamic equations can be used to compute results instead of the equations of motion obtained previously (Eq. (5) to Eq. (9)). This adjustment permits much quicker integration speeds, which saves energy and time. This can be done by substituting the time for the dimensionless time represented by τ. Equations (18) and (20) show the dimensionless time expression and the dimensionless frequency ω_0 formulation, where k_0 is the stiffness coefficient in the scenario where all the stiffness elements are the same and I_0 is the linearization of the parameter $I_E(\phi_n)$.

$$\tau = \omega_0 t. \tag{18}$$

$$\omega_0 = \sqrt{\frac{k_0(I_L + I_0)}{I_L I_0}}. \tag{19}$$

$$I_0 = I_c + m_1 r^2 + \frac{1}{2}(m_2 + m_p)r^2. \tag{20}$$

The equations of motion used for computing the results presented in this paper are the expressions 21, 22, 23, 24 and 25, each representing a different DOF. All the results obtained through them are in the domain of τ.

$$I_E(\phi_1)\omega_0^2{\phi_1}'' + \frac{dI_E(\phi_1)}{d\phi_1}\omega_0^2{\phi_1'}^2 + c_0\omega_0(\phi_1' - \phi_2') + c_E\omega_0{\phi_1}' + k_0(\phi_1 - \phi_2) = -M_d(\phi_1) \tag{21}$$

$$I_E(\phi_2 - \gamma_2)\omega_0^2\phi_2'' + \frac{dI_E(\phi_2 - \gamma_2)}{d\phi_2}\omega_0^2{\phi_2'}^2 + c_0\omega_0(\phi_2' - \phi_1') + c_0\omega_0(\phi_2' - \phi_3') + c_E\omega_0\phi_2' + ...$$

$$... + k_0(\phi_2 - \phi_1) + k_0(\phi_2 - \phi_3) = -M_d(\phi_2 - \beta_2) \tag{22}$$

$$I_E(\phi_3-\gamma_3)\omega_0^2\phi_3'' + \frac{dI_E(\phi_3-\gamma_3)}{d\phi_3}\omega_0^2{\phi_3'}^2 + c_0\omega_0(\phi_3'-\phi_2') + c_0\omega_0(\phi_3'-\phi_4') + c_E\omega_0\phi_3' + ...$$

$$... + k_0(\phi_3-\phi_2) + k_0(\phi_3-\phi_4) = -M_d(\phi_3-\beta_3) \tag{23}$$

$$I_E(\phi_4-\gamma_4)\omega_0^2\phi_4'' + \frac{dI_E(\phi_4-\gamma_4)}{d\phi_4}\omega_0^2{\phi_4'}^2 + c_0\omega_0(\phi_4'-\phi_3') + c_0\omega_0(\phi_4'-\phi_5') + c_E\omega_0\phi_4' + ...$$

$$... + k_0(\phi_4-\phi_3) + k_0(\phi_4-\phi_5) = -M_d(\phi_4-\beta_4) \tag{24}$$

$$I_L\omega_0^2\phi_5'' + c_0\omega_0(\phi_5'-\phi_4') + c_L\omega_0\phi_5' + k_0(\phi_5-\phi_4) = C_0 + C_1\omega_0{\phi_5}' \tag{25}$$

3. RESULTS AND DISCUSSION

The results presented in this section were obtained by using the integration numerical algorithm known as the Runge-Kutta Fourth Order method. First, the parameter represented by C_0, which is the electric motor torque's curve y-intercept, was modified, and a critical number was selected so that the difference between two neighboring DOF(s) angular displacements was maximum. The parameter C_0 is related to the amount of energy the motor gives to the crankshaft, and particular C_0 values can produce critical conditions where the crankshaft needs to bear maximum stress. Once this critical C_0 is found, the system's dynamical behavior over time can be investigated.

It was decided to analyze a system where all the stiffness elements were the same and then the dimensionless motion equations (Eq. (21) to Eq. (25)) were integrated. The Runge-Kutta step used in this analysis was equal to 0.00418879. The initial conditions at the time the code was initialized were all equal to zero except for $\phi_1'(0)$, which was equal to 0.1. However, the algorithm was programmed to print the system's dynamical response to the resistive and generative torques only when the critical conditions were reached and, at this point, the initial conditions were not equal to zero. They were equal to the last condition the system was when the critical C_0 was achieved. For this reason, the graphs do not start at zero. Also, ϕ_1' does not present any measurement unit with it because the normalization process described previously removed its original dimension aspect.

Four relative amplitude parameters were investigated in order to examine the crankshaft torsional vibrations. They are $\Delta\phi_1 = \phi_1 - \phi_2$, $\Delta\phi_2 = \phi_2 - \phi_3$, $\Delta\phi_3 = \phi_3 - \phi_4$ and $\Delta\phi_4 = \phi_4 - \phi_5$. As explained before, mechanical vibration analysis becomes more crucial in cases where these amplitude parameters reach maximum levels, and these scenarios are considered critical. These situations happen when the system is excited in certain frequencies known as the resonance frequencies. For systems with low damping coefficients, these frequencies are close to the system's natural frequencies. The system's critical condition was achieved by varying C_0. This variation was held for two different alteration step values, which were 100 and 200. It was possible to conclude from the results that for different variation numbers, the critical conditions occurred for different levels of C_0. On the other hand, it was also possible to determine that no matter what the level of C_0 was, considering situations where the C_0 variations were different, the maximum amplitude for a certain DOF was always the same for the same maximum velocities. If the mechanical parameters such as the moments of inertia for each DOF and the stiffness and damping coefficients were maintained, the critical condition always happened for the same maximum velocity, independently of the C_0 variation chosen for the analysis. Figure 3 shows that for different C_0 variation steps, the critical condition represented by the curve's peak happens for different $C_0(s)$. On the other hand, Fig. 4 shows that for different C_0 variation steps, the critical condition happens for the same maximum velocity in a certain DOF. Both figures present results related to the first DOF.

Figure 5 shows all the $\Delta\phi$ amplitude curves, considering all the existing DOF(s). As it can be seen, the highest levels for each curve do not happen for the same C_0. In order to choose a number that could contemplate more DOF(s), it was decided to run the code for a C_0 number equal to 13300. This decision was taken since this number is precisely the level represented by the dashed vertical line presented in Fig. 5. As one can notice, $\Delta\phi_3$ curve's peak happens when C_0 is 13300. Moreover, it was considered an adequate decision to select this number since $\Delta\phi_2$ and $\Delta\phi_4$ critical C_0(s) are not too distant from this level.

Once this decision was taken, the code could be run for a chosen C_0 variation step number, and when the critical C_0 level was achieved for this specific step, a dynamical analysis could be held. A C_0 variation step equal to 200 was selected to take place in this investigation, and at the moment C_0 was 13300 and the selected critical condition was achieved the dynamical analysis occurred.

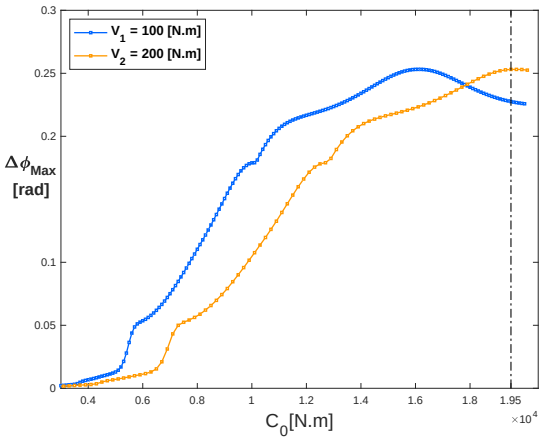

Figura 3: **Critical conditions for different C_0 step variations.**

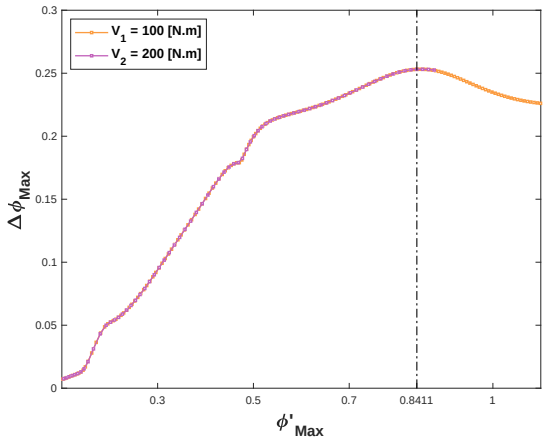

Figura 4: **Maximum velocity-amplitude curve for different C_0 step variations.**

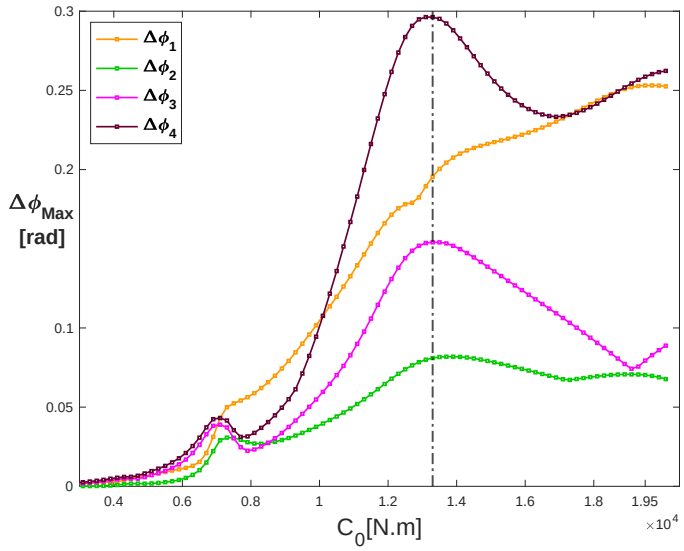

Figura 5: C_0 **vs** $\Delta\phi$ **curves for all the existing DOF(s).**

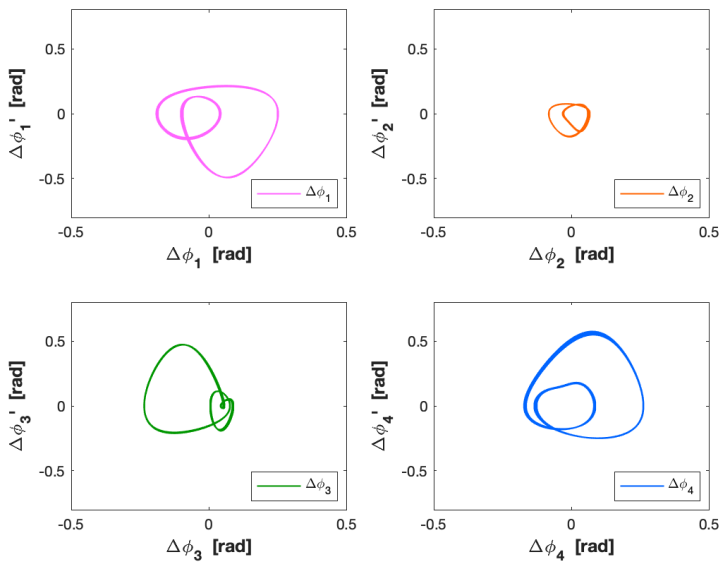

Figura 6: **Phase spaces for each** $\Delta\phi$**.**

The dynamic analysis was held for the elected C_0, and some results could be evaluated. Figure 6 presents the steady-state response in phase spaces for all the four $\Delta\phi$(s). The evaluated data represents the last 15% of the full information that was obtained. This decision was made to avoid data related to the transient stage. It can be seen that the torsional vibration amplitude is different for all different $\Delta\phi$(s). As it can be seen, there are differences in shape and size. The different shapes are related to the influence of nonlinearities. The more different from a circular shape the curve is, the stronger the influence of these nonlinearities. It is also interesting to notice in the Fig. 6 that the second $\Delta\phi$ is much smaller than the rest. It means velocities and angular displacements related to the second and the third DOF(s) are not so different from one another.

Last, Fig. 7 shows the frequencies that can be found when the dynamic response is analyzed in the frequency domain. The spectrum presents data for the four $\Delta\phi$(s). As it can be seen, the peaks happen in the same frequencies for all of them. A brief analysis of the numbers related to these peaks reveals that these values are multiples of the rotating frequency. The variable inertia not only adds a nonlinear aspect to the model but also works in a way that unbalances the shaft and causes torsional vibrations. The nonlinearities are responsible for the presence of the more frequency components, as can be seen in Fig. 7.

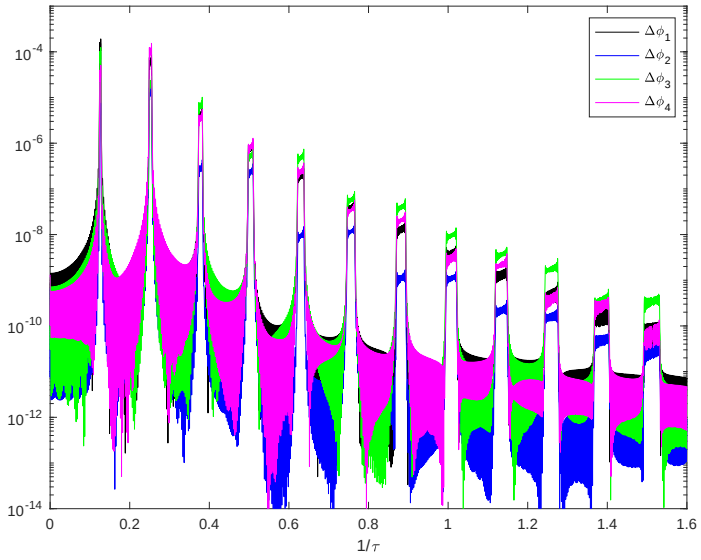

Figura 7: **Frequencies related to the rotating frequency and their multiples.**

4. CONCLUSION

This study presented a nonlinear model for a compressor with four cylinders and an electric motor, totalizing five degrees of freedom. The nonlinear characteristic comes from the variable inertia aspect the slider-crank mechanisms related to the cylinders have. It was possible to investigate which value of C_0 would result in a critical condition in order to analyze how the system would act dynamically. It was possible to identify the influence nonlinearities have on this model since the phase spaces presented distinct shapes, very different from what is expected in linear models. It was also possible to notice their influence on the frequency components as, not only the rotating frequency appeared in the frequency domain analysis but also its multiples were found.

5. REFERENCES

Aliakbari, K., Safarzadeh, N. and Mortazavi, S., 2018. "Analysis of the crankshaft failure of wheel loader diesel engine". Vol. 31, pp. 473–479. doi:10.5829/ije.2018.31.03c.10.

Brusa, E., Delprete, C. and Genta, G., 1997. "Torsional vibration of crankshafts: Effects of non-constant moments of inertia". Vol. 205, pp. 135–150. doi:https://doi.org/10.1006/jsvi.1997.0964.

Dinca, L., Aldemir, T. and Rizzoni, G., 1999. "Fault detection and identification in dynamic systems with noisy data and parameter/modeling uncertainties". *Reliability Engineering System Safety*, Vol. 65, pp. 17–28. doi: https://www.sciencedirect.com/science/article/pii/S0951832098000775.

Doughty, S., 1988. *Mechanics of Machines*. Wiley, 1st edition.

Heywood, J.B., 1998. *Internal Combustion Engine Fundamentals*. McGraw-Hill.

Huang, Y., Yang, S. and Zhang, F., 2012. "Non-linear torsional vibration characteristics of an internal combustion engine crankshaft assembly." Vol. 25, p. 797–808. doi:https://doi.org/10.3901/CJME.2012.04.797.

Lyshevski, S.E., 2000. "Energy conversion and optimal energy management in diesel–electric drivetrains of hybrid-electric vehicles". *Energy Conversion and Management*, Vol. 41, pp. 13–24. doi:https://doi.org/10.1016/S0196-8904(99)00087-4.

Metallidis, P. and Natsiavas, S., 2003. "Linear and nonlinear dynamics of reciprocating engines". *International Journal of Non-linear Mechanics*, Vol. 38, pp. 723–738. doi:10.1016/S0020-7462(01)00129-9.

Nisbeth, J.K. and Budynas, R.G., 1989. *Shigley's Mechanical Engineering Design*. McGraw-Hill, 5th edition.

Pasricha, M.S. and Carnegie, W., 1979. "Formulation of the equations of dynamic motion including the effects of variable inertia on the torsional vibrations in reciprocating engines, part i". *Journal of Sound and Vibration*, Vol. 66, pp. 181–186. doi:https://doi.org/10.1016/0022-460X(79)90664-3.

Pesce, C.P., Tannuri, E.A. and Casetta, L., 2006. "The lagrange equations for systems with mass varying explicitly with position: some applications to offshore engineering". *Journal of the Brazilian Society of Mechanical Sciences and Engineering [online]*, Vol. 28, pp. 496–504. doi:10.1590/S1678-58782006000400015.

Wachel, J. and Tison, J., 1994. "Vibrations in reciprocating machinery and piping systems". p. 127–151.